AIAA JOURNAL
Vol. 38, No. 7, July 2000

Passively Damped Laminated Piezoelectric Shell Structures with Integrated Electric Networks

Dimitris A. Saravanos*
Ohio Aerospace Institute, Cleveland, Ohio 44142

Multifield mechanics are presented for curvilinear piezoelectric laminates interfaced with distributed passive electric components. The equations of motion for laminated piezoelectric shell structures with embedded passive electric networks are directly formulated and solved using a finite element methodology. The modal damping and frequencies of the piezoelectric shell are calculated from the poles of the system. Experimental and numerical results are presented for the modal damping and frequency of composite beams with a resistively shunted piezoceramic patch. The modal damping and frequency of plates, open cylindrical shells, and cylindrical composite blades with piezoelectric-resistor layers are predicted and illustrate the dependence of piezoelectric damping on shunting resistance, structural shape, and curvature.

Nomenclature

$[A]$, $[B]$, $[D]$ = stiffness matrices of curvilinear laminate
$[C]$ = elastic stiffness tensor
c, $[C_c]$ = specific capacitance and capacitance matrix, respectively
$\boldsymbol{D}$ = electric displacement vector
$[\bar{E}]$, $[\hat{E}]$ = laminate piezoelectric matrices
$\boldsymbol{E}$ = electric field vector
$[e]$ = piezoelectric tensor
$\{F\}$ = force
g^o_{11}, g^o_{22} = components of the metric tensor for reference surface A_0
H = electric enthalpy
h = laminate thickness
J = electric flux (or current density)
$[K]$ = stiffness matrices
k = curvature caused by flexure
$[M]$ = mass matrix
N = in-plane interpolation functions
$\{Q\}$ = electric charge
R_1, R_2 = local curvature radi along ξ and η axes
r, $[R_c]$ = specific resistance and resistance matrix, respectively
$\boldsymbol{S}$ = engineering strain
T = kinetic energy
t = time
u, v, w = displacements in curvilinear system along ξ, η, and ζ axes, respectively
x, y, z = global Cartesian coordinate system
β_ξ, β_η = rotation angles caused by flexure
$[\varepsilon]$ = electric permittivity tensor
ζ_k = modal damping ratio
ξ, η, ζ = curvilinear axes
ρ^A, ρ^B, ρ^D = laminate densities
$\boldsymbol{\sigma}$ = stress vector
ϕ = electric potential
Ψ^m = through-thickness interpolation function
ω = frequency

Subscripts

c = passive circuit
L = laminate
uu = elastic
$u\phi$ = piezoelectric
$\phi\phi$ = dielectric
, = differentiation

Superscripts

A = active electric potential component
E = constant electric field conditions
i, j = finite element node
m, n = points at beginning and end of discrete layers; also generalized variables
o = displacement on reference surface A_0
P = passive electric potential component
S = constant strain conditions

Introduction

THE continuous requirements imposed on many new structural applications for improved vibroacoustic response and weight reduction mandate the development of new damping concepts. Embedded piezoelectric layers introduce the unique capability to convert strain energy to electric energy during a vibration cycle and vice versa. By connecting passive electric networks of resistors and capacitors to the piezoelectric layers, a fraction of electric energy may be dissipated or spontaneously stored, thus increasing the damping and changing the natural frequencies of the structure. Compared to other techniques that typically introduce high damping, for example, the constrained interlaminar viscoelastic layer and active damping techniques, the passive piezoelectric damping can exhibit very desirable characteristics, such as capability to be modified, spontaneously or periodically, by tuning the properties of the passive electric elements (resistors, capacitors, etc.) as required, for example, in the case of vibration caused by a tonal disturbance; damping improvement may not decrease laminate stiffness, as is the case with viscoelastic damping layers; and the required hardware is minimal and may be even encapsulated into the laminate, thus adding minimal weight to the structure. Consequently, the approach may be very suitable for damping vibrations in rotating or moving components, such as turbomachinery blades, helicopter blades, and so forth.

Although substantial work has been reported in the area of active vibration control as described in recent reviews,[1,2] most of the reported work on passive piezoelectric damping has been limited to simple laminate and structural (mostly beam and plate) configurations. Hagood and von Flotow[3] were the first to study analytically and experimentally the use of passive piezoelectric elements to dampen beam structures. They presented admissible constitutive relations for piezoelectric layers connected to a shunting resistor, which were further specialized for the case of uniaxial loading and implemented on single-degree-of-freedom

Received 9 December 1998; revision received 2 December 1999; accepted for publication 4 December 1999. Copyright © 2000 by the American Institute of Aeronautics and Astronautics, Inc. All rights reserved.

*Senior Research Associate, 22800 Cedar Point Road; currently Assistant Professor, Department of Mechanical Engineering and Aeronautics, University of Patras, 265 00 Patras, Greece. Senior Member AIAA.

mass-spring systems. This model was used to analyze the damping performance of shunted piezoelectrics, to establish the relationship between damping, resistance, and other critical parameters, and to predict added modal damping on beams with shunted piezoelectric elements as the fraction of dissipated and maximum stored strain energy. The possibility to maximize the modal damping of beams by tuning the shunting resistance was illustrated for the first time both experimentally and analytically using energy estimations provided by a Ritz model. Law et al.[4] reported simplified models and experimental results for piezoelectric materials shunted by a load resistor. Davis and Lesieutre[5] predicted the passive damping of beams with resistively shunted piezoelectric patches using a finite element based strain energy dissipation approach, analyzed the phenomenon of resistance tuning for maximum damping, and reported analytical and experimental results. Koshigoe and Murdock[6] reported a simplified analytical formulation for plates with passive piezoelectric elements. Wang et al.[7] reported work on a semiactive vibration control approach for beams with piezoelectric elements combining passive electric components with an active controller concept. Yarlagadda et al.[8] presented micromechanics and experimental results for composites with resistively shunted piezoceramic fibers. Saravanos[9] developed laminate models for plates with resistively shunted piezoelectric layers and reported an exact in-plane Ritz formulation for the prediction of damping in composite plates with resistively shunted piezoelectric layers.

Although the reported work has provided valuable insight regarding the potential of passive piezoelectric damping, it has been mostly limited to beam and/or plate structures. This paper presents efficient mechanics and a finite element formulation for predicting damping in piezoelectric shell structures of arbitrary geometry and laminate configurations. The new elements of the method include 1) multifield mechanics for curvilinear composite laminates with piezoelectric layers attached to distributed passive electric components and 2) an associated shell finite element for directly predicting the modal damping, modal frequencies, and dynamic response of such damped piezoelectric shells. The laminate mechanics combine single-layer kinematic assumptions for the displacements with a layerwise variation of the electric potential. The formulation inherently considers the presence of distributed electric networks, thus enabling coupled and efficient representations of the integrated laminate-electric circuit system. The governing equations of motion of a piezoelectric composite shell with passive electric networks are described and solved in state-space form. The modal damping is explicitly calculated from the poles of the coupled structural system, rather than using the dissipated strain energy approach. The damped frequency response is directly calculated from the equations of motion.

Doubly Curved Piezolaminates with Passive Electric Networks

The curvilinear laminate configuration with attached distributed electric components and piezoelectric actuators is shown schematically in Fig. 1a. The assumption is made that each ply of the laminate remains parallel to a reference curvilinear surface A_0, which is defined with respect to a global Cartesian coordinate system $Oxyz$. An orthogonal curvilinear coordinate system $\bar{O}\xi\eta\zeta$ is defined, such that the axes ξ and η lie on the curvilinear reference surface A_0, while the axis ζ remains straight and perpendicular to the layers of the laminate. A series of resistor–capacitor circuits may be connected to piezoelectric layers.

Governing Material Equations

Each ply is assumed to be a linear piezoelectric material with properties defined on the orthogonal curvilinear system $\bar{O}\xi\eta\zeta$, with constitutive equations of the following form:

$$\boldsymbol{\sigma}_i = C_{ij}^E \boldsymbol{S}_j - e_{ik}\boldsymbol{E}_k, \qquad \boldsymbol{D}_l = e_{lj}\boldsymbol{S}_j + \varepsilon_{lk}^S \boldsymbol{E}_k \tag{1}$$

where $i, j = 1, \ldots, 6$ and $k, l = 1, \ldots, 3$; $\boldsymbol{\sigma}_i$ and $\boldsymbol{S}_i$ are the mechanical stresses and engineering strains in vectorial notation; $\boldsymbol{E}_k$ is the electric field vector; $\boldsymbol{D}_l$ is the electric displacement vector; C_{ij} is the elastic stiffness tensor; e_{lj} is the piezoelectric tensor; and ε_{lk} is the electric permittivity tensor of the material. The axes 1, 2, and 3 of the material are parallel to the curvilinear axes ξ, η, and ζ. The materials are assumed to be monoclinic class 2 crystals with a polarization axis parallel to the ζ axis and can be subject to an in-plane

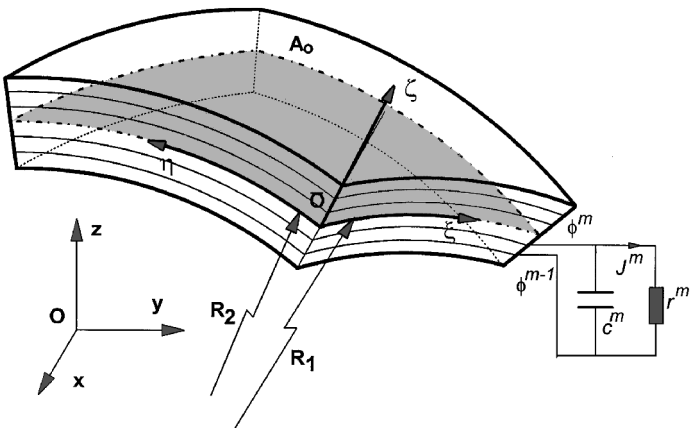

a) Geometry

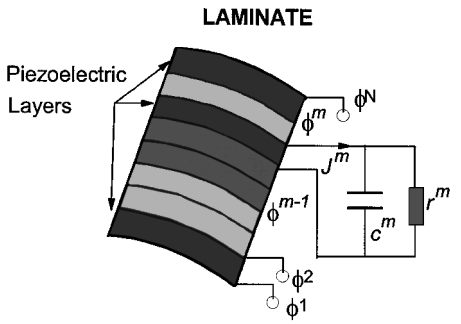

b) Through-thickness configuration

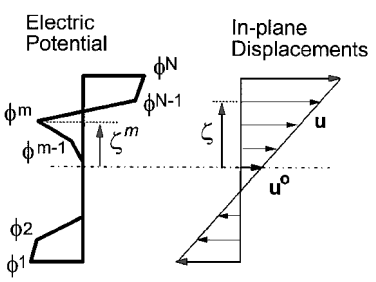

c) Assumed fields for electric potential and in-plane displacements

Fig. 1 Curvilinear piezoelectric laminate with embedded passive electric networks.

rotation (see Appendix for tensor definition). The strain and electric field components in the curvilinear coordinate system are related to the displacements and electric potential, respectively, as well as to the local radii of curvature and the components of the metric tensor. For a doubly curved laminate these relationships are not simple and are described in Ref. 10.

Laminate Theory

The mixed-field laminate theory[10] is extended here to address the case of piezoelectric laminates with distributed electric circuitry (Fig. 1b). The theory combines linear displacement fields through the thickness of the laminate for the displacements u, v (along the ξ and η axes, respectively) with a layerwise electric potential field through the laminate, consisting of N discrete continuous segments (Fig. 1c). By assuming different approximations for each field, the method retains computational efficiency for thin and intermediate thick laminates, while maintaining the representation of multiple fields and piezoelectric coupling. The discrete-layer assumption effectively subdivides the laminate into $(N-1)$ sublaminates (or discrete layers). The grade of subdivision can be arbitrarily controlled according to the configuration of the piezoelectric layers and/or the required detail of approximation. A continuous electric potential is assumed in each sublaminate, such that a C_0 piecewise continuous variation results through the thickness of the laminate. The displacements and electric potential take the following form:

$$\begin{aligned} u(\xi, \eta, \zeta, t) &= u^o(\xi, \eta, t) + \zeta\beta_\xi(\xi, \eta, t) \\ v(\xi, \eta, \zeta, t) &= v^o(\xi, \eta, t) + \zeta\beta_\eta(\xi, \eta, t) \\ w(\xi, \eta, \zeta, t) &= w^o(\xi, \eta, t) \\ \phi(\xi, \eta, \zeta, t) &= \sum_{m=1}^{N} \phi^m(\xi, \eta, t)\Psi^m(\zeta) \end{aligned} \tag{2}$$

where u^o, v^o, w^o are displacements on the reference surface A_0; ϕ^m is the electric potential at each point ζ^m (see Fig. 1c); and $\Psi^m(\zeta)$ are interpolation functions. The resultant generalized compatibility equations are shown in the Appendix.

Equations of Motion

The variational statement of the equations of motion for a piezoelectric laminate with assumed displacement and electric potential fields takes the form[10]

$$\int_{A_0} -[\delta H_L(\boldsymbol{S}, \boldsymbol{E}) - \delta T_L]\,\mathrm{d}\xi\,\mathrm{d}\eta + \oint_{\Gamma_\tau} \delta u_i^T\, \bar{\tau}_i\,\mathrm{d}\Gamma + \oint_{\Gamma_D} \delta\phi\,\bar{D}\,\mathrm{d}\Gamma = 0 \tag{3}$$

where A_0 is the curvilinear reference surface, τ and $\bar{D}$ are the surface tractions and electric displacement acting, respectively, on boundary surfaces Γ_τ, Γ_D; and δH_L and δT_L are the variations of the electric enthalpy and kinetic energy of the laminate, defined as

$$\langle \delta H_L, \delta T_L \rangle = \int_0^h \langle \delta H, \delta T \rangle g_{11}^o g_{22}^o\,\mathrm{d}\zeta \tag{4}$$

The electric enthalpy of the piezoelectric laminate is a quadratic expression of the generalized strain/electric field and the generalized laminate matrices[10]:

$$\begin{aligned} \delta H_L &= \delta \boldsymbol{S}_i^o A_{ij} \boldsymbol{S}_j^o + \delta \boldsymbol{S}_i^o B_{ij} k_j + \delta k_j B_{ji} \boldsymbol{S}_i^o + \delta k_i \boldsymbol{D}_{ij} k_j \\ &\quad - \sum_{m=1}^{N} \left(\delta \boldsymbol{S}_i^o \bar{E}_{ik}^m \boldsymbol{E}_k^m + \delta \boldsymbol{E}_k^m \bar{E}_{ki}^m \boldsymbol{S}_i^o + \delta k_j \hat{E}_j^m \boldsymbol{E}_3^m + \delta \boldsymbol{E}_3^m \hat{E}_j^m k_j \right) \\ &\quad - \sum_{m=1}^{N} \sum_{n=1}^{N} \delta \boldsymbol{E}_k^m G_{kl}^{mn} \boldsymbol{E}_l^m \end{aligned} \tag{5}$$

In the preceding equation, $[\bar{E}^m]$ and $[\hat{E}^m]$ are laminate piezoelectric matrices representing the resultant average forces and moments, respectively, which will act on the laminate cross section caused by the generalized applied electric field, and $[G^{mn}]$ are the laminate matrices of electric permittivity (see Appendix). The kinetic energy of the laminate takes the form

$$\delta T_L = \delta u_i^o \rho_i^A \ddot{u}_i^o + \delta u_j^o \rho_j^B \dot{\beta}_j + \delta\beta_j \rho_j^B \ddot{u}_j + \delta\beta_j \rho_j^D \dot{\beta}_J \qquad i = 1, \ldots, 3, \quad j = 1, 2 \tag{6}$$

where $u_i^o = \{u^o, v^o, w^o\}$ and $\beta_i = \{\beta_\xi, \beta_\eta\}$; ρ^A, ρ^B, ρ^D are the generalized densities, expressing the mass, mass coupling, and rotational inertia per unit area, respectively, of the laminate.

Electric Circuitry

Considering that a passive electric circuit with resistive and capacitive elements is interfaced to the terminal surfaces m and n (see Fig. 1b) of the piezoelectric laminate, the electric potential ϕ and electric flux (or current density) J in the circuit are related as follows:

$$\begin{Bmatrix} J^m \\ J^n \end{Bmatrix} = \begin{pmatrix} c & -c \\ -c & c \end{pmatrix} \begin{Bmatrix} \dot{\phi}^m \\ \dot{\phi}^n \end{Bmatrix} + \begin{bmatrix} r^{-1} & -r^{-1} \\ -r^{-1} & r^{-1} \end{bmatrix} \begin{Bmatrix} \phi^m \\ \phi^n \end{Bmatrix} \tag{7}$$

Considering the more general case of multiple passive networks attached at various thickness locations, the equilibrium equations are expressed in similar matrix form:

$$\{J_c(t)\} = [c]\{\dot{\phi}_c(t)\} + [r^{-1}]\{\phi_c(t)\} \tag{8}$$

where the specific capacitance and resistance matrices are formulated in accordance with Eq. (7) and include contributions of all laminate circuits.

Electrical Compatibility Conditions

At the j common terminal between the piezoelectric laminate and the electric circuit, the electric potential at the laminate should be equal to the electric potential of the circuit, and the electric flux in the electric circuit should be equal to the rate of the generalized normal electric displacement:

$$\phi_L^m = \phi_c^m, \qquad J_c^m = \dot{D}_{3L}^m \tag{9}$$

Passive Piezoelectric Shell Structures

A finite element based method is developed using the preceding laminate mechanics for predicting the dynamic characteristics and response of shell structures having piezoelectric layers or patches attached to passive electric circuits. The finite element method (FEM) uses local approximations of the generalized electromechanical state (displacements, rotation angles, and electric potential) on the reference surface A_0 of the following type:

$$\begin{aligned} &\langle u^o(\xi, \eta, t), v^o(\xi, \eta, t), w^o(\xi, \eta, t) \rangle \\ &\quad = \sum_{i=1}^{M} \langle u^{oi}(t), v^{oi}(t), w^{oi}(t) \rangle N^i(\xi, \eta) \\ &\langle \beta_\xi(\xi, \eta, t), \beta_\eta(\xi, \eta, t) \rangle = \sum_{i=1}^{M} \langle \beta_\xi^i(t), \beta_\eta^i(t) \rangle N^i(\xi, \eta) \\ &\phi^m(\xi, \eta, t) = \sum_{i=1}^{M} \phi^{mi}(t) N^i(\xi, \eta), \qquad m = 1, \ldots, N \end{aligned} \tag{10}$$

where superscript m indicates the nodal generalized state variable corresponding to the in-plane interpolation function $N^i(\xi, \eta)$ of the ith node. Using this framework, an eight-node quadrilateral curvilinear element was developed in this work, which enables modeling of both the piezoelectric structure and the distributed electric circuitry.

Piezoelectric Structure

Substituting Eqs. (10) into the generalized equations of motion (3) and collecting the coefficients as mandated by Eqs. (5) and (6),

the governing dynamic equations of the piezoelectric structure are expressed in discrete matrix forms.[10] Selective reduced integration is used in the calculation of shear stiffness and piezoelectric terms to eliminate spurious stiffening observed at low thicknesses.

An active–passive piezoelectric structure is considered, which may contain piezoelectric layers connected to passive circuitry, as well as piezoelectric actuators (i.e., piezoelectric layers with applied electric potential). In this case the electric potential vector can be subdivided in a passive component ϕ^p representing the electric potential at passive piezoelectric layer nodes and an active component ϕ^A representing the potential imposed on the actuator nodes, such that $\{\phi\} = \{\phi^P; \phi^A\}$. The discrete system of equations is partitioned to the following form:

$$\begin{pmatrix} [M_{uu}] & 0 \\ 0 & 0 \end{pmatrix} \begin{Bmatrix} \{\ddot{u}\} \\ \{\ddot{\phi}^P\} \end{Bmatrix} + \begin{bmatrix} [K_{uu}] & [K_{u\phi}^{PP}] \\ [K_{\phi u}^{PP}] & [K_{\phi\phi}^{PP}] \end{bmatrix} \begin{Bmatrix} \{u\} \\ \{\phi^P\} \end{Bmatrix} = \begin{Bmatrix} \{F(t)\} - [K_{u\phi}^{PA}]\{\phi^A\} \\ \{Q^P(t)\} - [K_{\phi\phi}^{PA}]\{\phi^A\} \end{Bmatrix} \tag{11}$$

Submatrices K_{uu}, $K_{u\phi}$, and $K_{\phi\phi}$ indicate the elastic, piezoelectric, and permittivity matrices; M_{uu} is the mass matrix. $F(t)$ is the force vector containing surface tractions, body, and nodal forces; $Q^P(t)$ is the discretized electric charge vector containing surface electric displacements applied at passive piezoelectric layers. The left-hand side contains N_s unknown displacements $\{u\}$ and N_p unknown electric potentials $\{\phi^P\}$. The right-hand side contains the applied forces $F(t)$, electric charges $Q^P(t)$, and applied electric potential $\{\phi^A\}$ at the actuators. The presence of continuous electrodes on piezoelectric layers is considered in the preceding equation by imposing equality constraints on the unknown nodal electric potential over the electrode surface by means of the penalty method.

Electric Circuitry

Assuming that the free surface of passive piezoelectric layers Γ_D is effectively the interface surface between passive piezoelectrics and electric circuits, the applied electric displacement term in Eq. (3) can be rewritten considering the second compatibility equation (9):

$$\int_{\Gamma_D} \delta\phi \frac{\mathrm{d}\bar{D}}{\mathrm{d}t} \mathrm{d}\Gamma = \int_{\Gamma_D} \delta\phi J_c \, \mathrm{d}\Gamma \tag{12}$$

The combination of Eq. (12) with Eq. (8) and the application of the layerwise and finite element approximations of electric potential yield the discretized compatibility equation for the electric flux between the piezoelectric layers and passive electric circuitry

$$\{\dot{Q}^p(t)\} = \{I_c(t)\} = [C_c]\{\dot{\Phi}_c(t)\} + [R_c^{-1}]\{\Phi_c(t)\} \tag{13}$$

where $\{I_c\}$ is the current vector in electric circuitry. The capacitance and inverse resistance submatrices of the distributed electric system, between nodes i, j of the finite element, are, respectively,

$$[R_c^{-1}]^{ij} = \int_{\Gamma_D} [N^i]^T [r^{-1}][N^j] g_{11}^o g_{22}^o \, \mathrm{d}\xi \, \mathrm{d}\eta$$

$$[C_c]^{ij} = \int_{\Gamma_D} [N^i]^T [c][N^j] g_{11}^o g_{22}^o \, \mathrm{d}\xi \, \mathrm{d}\eta \tag{14}$$

Combined Structural System

Combining the equations of motion for the piezoelectric shell (11) with the compatibility equation (13) for the distributed electric system and recognizing from the first compatibility equation (9) that $\{\Phi_c\}$ is equal to the passive electric potential component $\{\Phi^p\}$, the governing equations of the combined system result in state-space form. The left-hand side includes the unknown electromechanical state $\{V; U; \Phi^p\}$, which contains the velocities, displacements, and the electric potential at the common terminals of the passive piezoelectric layers. The right-hand side includes the excitation of the plate in terms of mechanical loads and applied voltages on the actuators:

$$\begin{bmatrix} [M_{uu}] & 0 & 0 \\ 0 & I & 0 \\ 0 & 0 & [K_{\phi\phi}^{PP}] - [C_c] \end{bmatrix} \begin{Bmatrix} \{\dot{V}\} \\ \{\dot{U}\} \\ \{\dot{\Phi}^p\} \end{Bmatrix} = \begin{bmatrix} 0 & -[K_{uu}] & -[K_{u\phi}^{PP}] \\ I & 0 & 0 \\ [-K_{\phi u}^{PP}] & 0 & [R_c^{-1}] \end{bmatrix} \begin{Bmatrix} \{V\} \\ \{U\} \\ \{\Phi^p\} \end{Bmatrix} + \begin{Bmatrix} \{F(t)\} - [K_{u\phi}^{PA}]\{\Phi^A\} \\ 0 \\ 0 \end{Bmatrix} \tag{15}$$

The capacitance $[C_c]$ of the electric circuit is added to the internal capacitance of the passive piezoelectric layers. This capacitance matrix effectively modifies the capacitance of the system; thus it may be used to alter the time constants in the resistance–capacitor circuits formed by the piezoelectric layer capacitance and the shunt resistor. The shunt resistance appears to provide the only damping mechanism because no other sources of damping are considered in the present study.

Modal Characteristics

Assuming free-vibration conditions with state variables of the form $\{U(t), V(t), \Phi^P(t)\} = \{U, V, \Phi^P\}e^{st}$, $2N_s + N_p$ complex eigenvalues (poles) are calculated from Eq. (15). The $2N_s$ poles are conjugate complex pairs s_k^* corresponding to the vibration modes. The remaining N_p eigenvalues are negative real numbers corresponding to time constants of the electric circuitry. The modal frequency and damping ratio of the structural modes are directly calculated from the poles:

$$\omega_k = \left\| s_k^* \right\|, \qquad \zeta_k = Re\left(s_k^*\right) / \omega_k \tag{16}$$

Frequency Response

Assuming harmonic state variables $\{U(t), V(t), \Phi^P(t)\} = \{U, V, \Phi^P\}e^{j\omega t}$, force $Fe^{j\omega t}$, and applied electric potential $\Phi^A e^{j\omega t}$, Eq. (15) provides a linear system of equations with complex coefficients. Solution of the system yields the response $\{U, V, \Phi^P\}$ of the structure at frequency ω.

Case Studies

Various numerical studies were performed to evaluate the accuracy and convergence of the developed formulation, including 1) comparisons with measured damping and frequency data of composite beams with an attached piezoceramic-resistor patch and 2) convergence studies toward exact Ritz in-plane solutions for specialty plates and cylindrical panels with distributed piezoelectric-resistor layers. The piezoelectric damping of clamped-free cylindrical composite blades with discrete piezoelectric-resistor patches was also investigated.

Materials and Assumptions

The properties of all materials are shown in Table 1. The T300/934 graphite/epoxy composite was used for all composite laminates in this work. Composite beam specimens of this material were also fabricated and tested. A PZT-4 piezoceramic was considered in all numerical examples. PZT-4 patches provided by American Piezoceramics International (material APC 840) were used in the fabrication of the beam specimens.

$[0_4/90_4]_s$ Cantilever Beam

A $[0_4/90_4]_s$ T300/934 graphite/epoxy beam, 234 mm long and 25.4 mm wide, with a surface epoxied PZT-4 patch having a variable resistor attached on its surface terminals was fabricated and tested. The beam was supported in cantilever configuration, and the modal characteristics were measured and also predicted using the developed shell finite element. Figure 2 shows the geometry and testing configuration of the beam. The direction of fibers in

the 0-deg plies was parallel to the beam axis, the thickness of each composite ply was 0.262 mm, and the thickness of the piezoceramic patch was 0.762 mm. The size of the piezoceramic patch was 50.8 by 25.4 mm, and the lower electrode was wrapped around the free edge and covered 2 mm of the upper surface to provide space for the wiring attachment (see Fig. 2).

The beam was impacted with an instrumented hammer, and the acceleration was measured using a 0.50-g accelerometer, at the location shown in Fig. 2. The electric signals from the impact hammer and accelerometer were acquired and digitized using a PC-based dynamic data acquisition card and software. The frequency response functions were calculated from the impact response data using fast Fourier transform software. The poles of the beam were subsequently estimated using the method of complex exponentials. A model transfer function consisting of a series of conjugate pairs of complex exponential terms (each pair corresponding to a mode) was correlated to the measured frequency response function until the least-squares error was minimized. The modal frequency and damping were subsequently calculated from the poles of the model system, and they were assumed to approximate closely the modal damping and frequency values of the tested beam. After each measurement the resistance was varied and measured, and the test was repeated.

The measured damping increment and natural frequency of the first mode of the beam for various resistance values are shown in Figs. 3 and 4. The damping increment was calculated from the measured damping at resistance R by subtracting the measured damping at open circuit conditions ($R = \infty$), which was considered to represent the baseline damping of the beam. The same figures also show the predicted values using a 14×1 nonuniform mesh of the shell finite element. The presence of continuous electrodes was also modeled. The mass of the accelerometer was found to affect the dynamics of the beam and was included in the FEM. Both measured and predicted damping and frequency values follow the same trends and are within reasonable agreement. The finite element predictions seem to overestimate the measured data. The lower measured values are attributed to the presence and compliance of the adhesive layer (whereas the present formulation assumes a perfect bond) and possible degradation of the actual piezoelectric coefficients than the ones provided by the manufacturer and used in the model.

Table 1 Mechanical properties ($\varepsilon_0 = 8.85 \times 10^{-12}$ F/m, electric permittivity of air)

Property	Composite T300/934	PZT-4
Elastic properties		
E_{11}, GPa	132.4	81.3
E_{22}, GPa	10.8	81.3
E_{33}, GPa	10.8	64.5
G_{23}, GPa	3.6	25.6
G_{13}, GPa	5.6	25.6
G_{12}, GPa	5.6	30.6
ν_{12}	0.24	0.33
ν_{13}	0.24	0.43
ν_{23}	0.49	0.43
Piezoelectric coefficients (10^{-12} m/V)		
d_{31}	0	−122
d_{32}	0	−122
d_{24}	0	495
d_{15}	0	495
Electric permittivity		
$\varepsilon_{11}/\varepsilon_0$	3.5	1475
$\varepsilon_{22}/\varepsilon_0$	3.0	1475
$\varepsilon_{33}/\varepsilon_0$	3.0	1300
Mass density ρ(kg/m^3)		
——	1578	7600

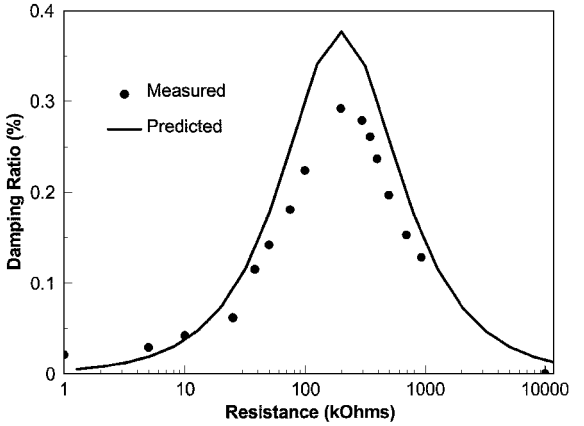

Fig. 3 Increase in the first mode damping of a $[0_4/90_4]_s$ T300/934 beam for various resistance values.

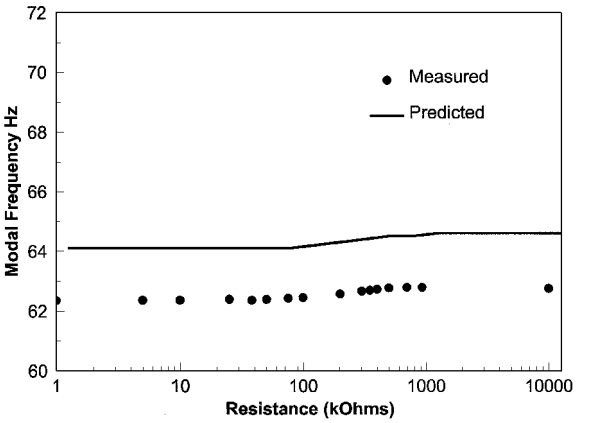

Fig. 4 Effect of resistance on the first modal frequency of $[0_4/90_4]_s$ T300/934 beam.

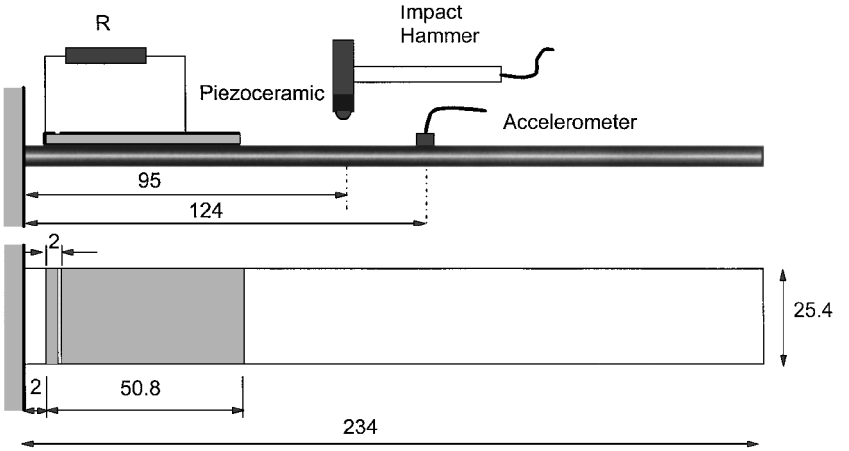

Fig. 2 $[0_4/90_4]_s$ T300/934 cantilever beam with attached PZT-4 resistor patch: side and top views (dimensions in millimeters).

Figures 3 and 4 illustrate that there is an optimal resistance where damping reaches a maximum and frequency shifts to a higher value. This relationship between modal damping, shunt resistance, capacitance of the piezoelectric and modal frequency was observed and analyzed in the works of Hagood and von Flotow[3] and Davis and Lesieutre,[5] who also reported results for higher beam modes. In summary, beyond this optimal resistance value, the resistor and the capacitance of the piezoelectric layer effectively form a low-pass filter on the electric current flowing through the resistor. The cutoff frequency is related to the resistance and capacitance of the piezoelectric layers. When the cutoff frequency exceeds the frequency of a specific vibration mode, the electric flux through the resistor decreases, and a fraction of electric flux is stored in the piezoelectric capacitor during a vibration cycle. This decreases the dissipation of electric energy at the resistor, and thus lowers damping. As the bulk of electric energy remains stored in the piezoelectric capacitor, the elastic strain energy of the beam is reduced, resulting in higher natural frequencies.

Simply Supported Plate

A simply supported $[p/0/90/90/0/p]$ cross-ply graphite/epoxy composite square plate is considered, with surface attached distributed piezoceramic (PZT-4) layers, each grounded at the inner surface and shunted with equal distributed resistance per unit area r. The nominal thickness of each composite ply was $t_l = 0.375$ mm and of each piezoelectric layer was $t_p = 0.250$ mm, thus resulting in total plate thickness $h = 2$ mm. The free length of the plate along the x and y axes was $L_x/h = L_y/h = 157$. Considering the two planes of symmetry, only a quarter of the plate was modeled using a uniform finite element mesh. The finite element results are compared with an exact Ritz solution, which was developed using the same laminate theory assumptions.[9] The Ritz solution assumes Fourier trial functions, which, as shown in Ref. 9, satisfy the boundary conditions and governing equations for this type of problem, thus providing an exact in-plane solution for the corresponding mode shape, frequency, and damping. Figure 5 shows the damping and natural frequency finite element predictions of the fundamental mode using various mesh densities, together with the corresponding exact Ritz solution.[9] Both finite element damping and natural frequency predictions converge rapidly to the exact in-plane solution. As in the preceding example, there is an optimal resistance where damping reaches a maximum and frequency shifts to a higher value. Figure 6 shows the damping of additional modes evaluated using a 6×6 uniform mesh. Besides the good agreement between the finite element and exact solution, the results show that the corresponding damping peak occurs at lower resistance, as the modal frequency increases.

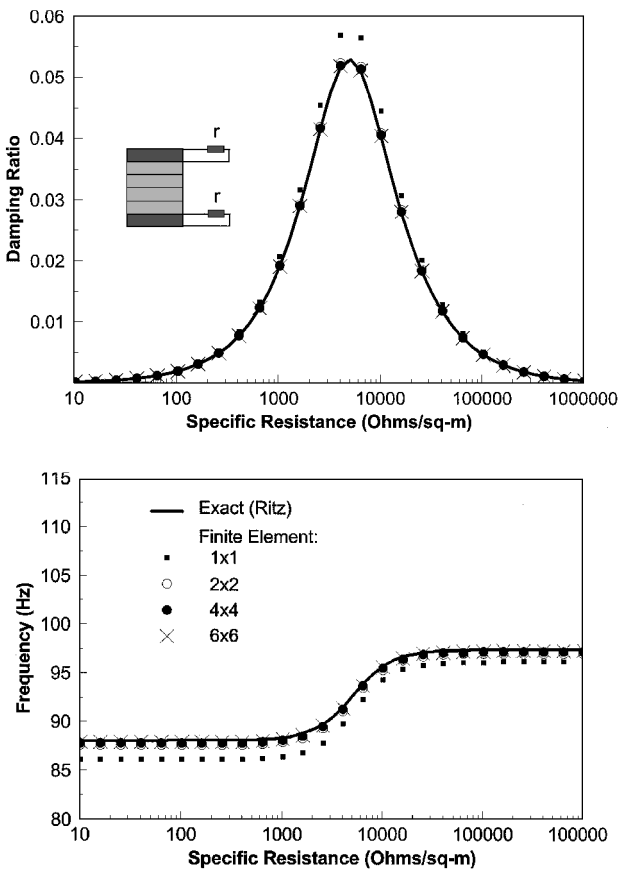

Fig. 5 Fundamental modal damping and frequency using various mesh densities for a $[p/0/90/90/0 \lhd p]$ graphite/epoxy square plate with PZT-4 layers connected to distributed specific resistance r.

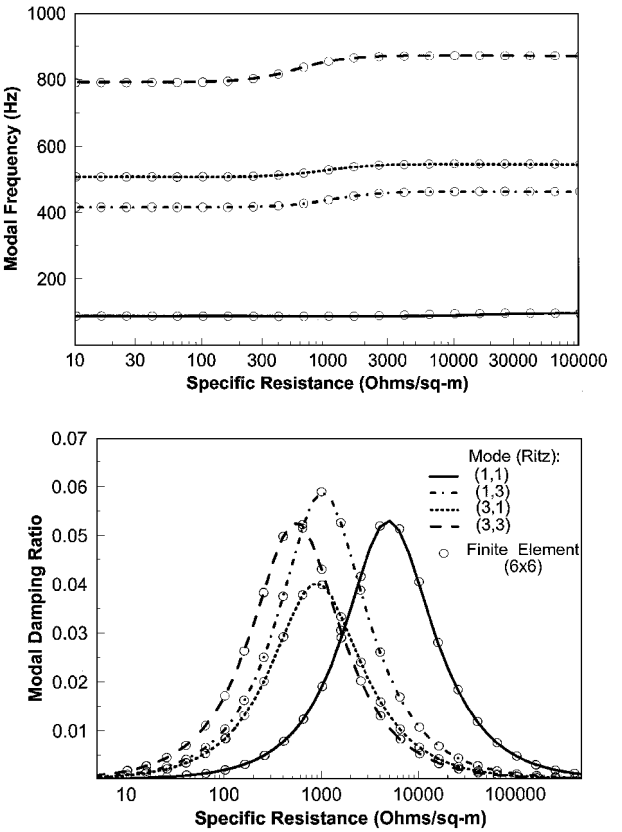

Fig. 6 Predicted damping and frequencies of the first four modes of a graphite/epoxy square plate with PZT-4 layers connected to distributed specific resistance r.

Simply Supported Cylindrical Panel

The simply supported cylindrical quarter panel shown in Fig. 7 is considered. The panel has identical graphite/epoxy $[p/0/90]_s$ laminate configuration, ply thicknesses, and materials with the preceding case, with the 0-deg plies aligned along the hoop direction. Each PZT-4 layer is shunted with a distributed resistance per unit area r. The length of the panel along the hoop (ξ) and axial (η) axes is $L_\xi/h = L_\eta/h = 157$. Taking into consideration the symmetry in axial direction, only one-half of the panel was modeled using a uniform mesh.

Figure 8 shows the damping and frequency of the first mode, which in this case is mode (3,1). The numbers in parenthesis indicate the semiwavelengths along the hoop (ξ) and axial (η) direction. Both damping and frequency predictions seem to rapidly converge toward an exact in-plane solution, although higher element subdivisions were required along the circumferential direction. Figure 9 shows the predicted damping and frequency corresponding to mode shape (1,1), which occurs at a higher natural frequency, as a result of stiffening from extension-bending coupling introduced by the curvature. The finite element predictions seem to converge to slightly different values from the Ritz solution. Figure 10 shows damping predictions for the first five modes, and the very good overall agreement between a 16×4 finite element mesh and an in-plane exact Ritz method developed by the author. All modes illustrate the familiar pattern of a maximum damping peak and shifting in the natural

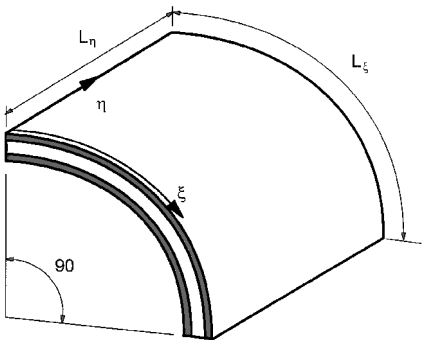

Fig. 7 Cylindrical [*p*/0/90/90/0/*p*] graphite/epoxy, PZT-4 quarter panel.

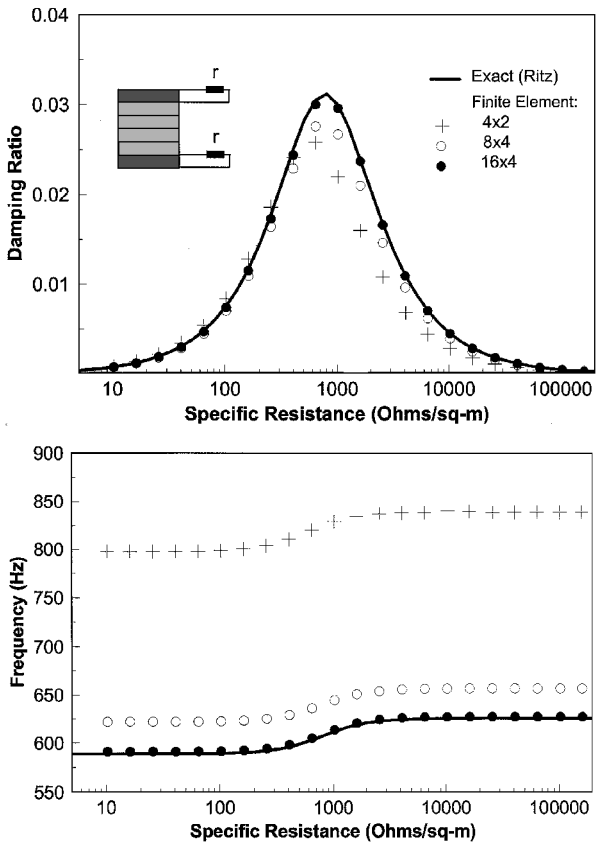

Fig. 8 Predicted damping and frequency of first frequency mode (3,1) using various mesh densities for the [*p*/0/90/90/0/*p*] graphite/epoxy cylindrical quarter panel (Fig. 7) with distributed specific resistance *r* connected to each PZT-4 layer.

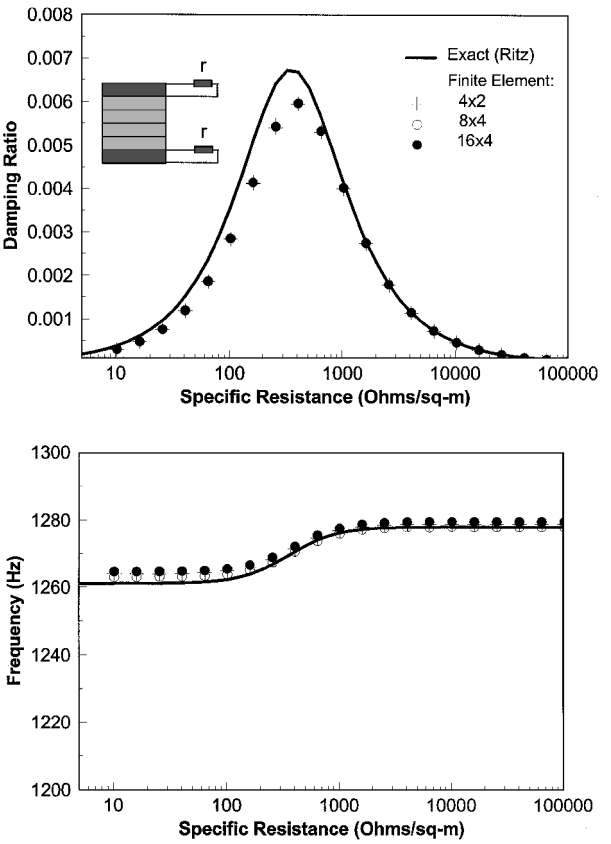

Fig. 9 Predicted damping and frequency of mode (1,1) using various mesh densities for the [*p*/0/90/90/0/*p*] graphite/epoxy cylindrical quarter panel (Fig. 7) with distributed specific resistance *r* connected to each PZT-4 layer.

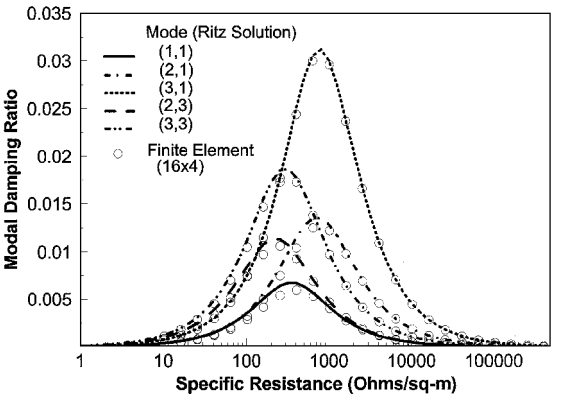

Fig. 10 Damping of various mode shapes for the [*p*/0/90/90/0/*p*] graphite/epoxy cylindrical quarter panel (Fig. 7) with distributed specific resistance *r* connected to each PZT-4 layer.

frequency with increasing resistance values. The prevailing difference with the preceding plate case is the wide variation between the damping peaks of the various modes, with modes (1,1) and (3,1) having the lower and higher damping peak, respectively. Curvature-induced extension-flexure coupling seems to affect adversely the damping effectiveness of the piezoelectric layers, as it reduces the flexural strain energy stored and dissipated at the piezoelectric layers. Overall, the present and preceding cases have demonstrated the accuracy and convergence rate of the developed approach.

Cantilever Cylindrical Panel with Piezoelectric Patches

The more realistic case of a $[0/90/45/-45]_s$ graphite/epoxy cylindrical quarter panel having curved PZT-4 patches symmetrically attached on both sides was also considered (Fig. 11). The 0-deg plies are parallel to the ξ axis. The thicknesses of each composite ply and PZT-4 patch are 0.375 and 0.500 mm, respectively, and the length aspect ratio was $L_\xi/L_\eta = 2$ and $L_\eta = 140$ mm. The panel was clamped at the lower curved edge and free at all others to resemble an untwisted cylindrical blade. The location of piezoelectric patches (shaded area) on each side and the finite element mesh are shown in Fig. 11. The surface terminals of each piezoceramic patch were assumed to be connected to an individual resistor; however, the values of the resistors were selected such that the specific resistance remained the same for all piezoceramic patches. The continuous electrodes were modeled using penalty equality constraints on the surface electric potential.

The predicted modal damping of the first five modes is shown in Fig. 12. Again the damping variation of each mode follows the familiar peak pattern as the resistance increases, yet the modal damping varies widely between various modes. Because of the finite size and continuous electrodes of the piezoelectric patches, their location and size become important parameters in connection with the respective mode shape. The present configuration seems to be more effective with flexural modes (modes 2, 4, and 5), while providing minimal damping for twisting modes (1 and 3). The lower damping values, compared to earlier cases of idealized distributed piezoelectric

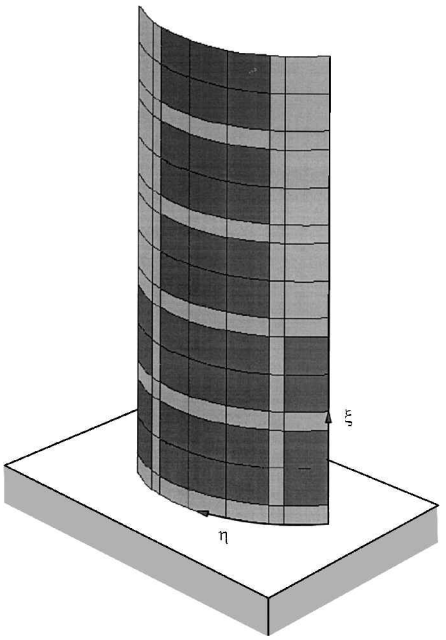

Fig. 11 Cylindrical $[0/90/45/-45]_s$ graphite/epoxy panel with symmetrically attached resistively shunted curved PZT-4 patches (shown as shaded areas) on both sides.

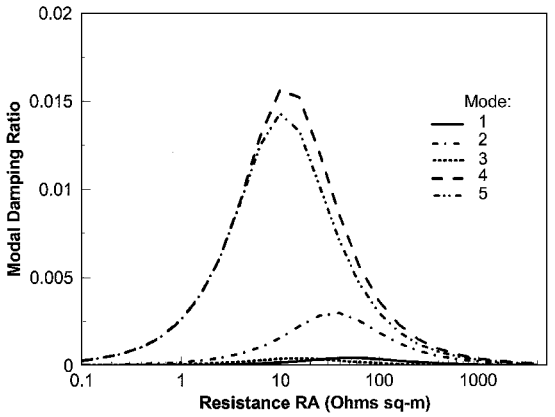

Fig. 12 Damping predictions for the first five modes of the cantilever cylindrical $[0/90/45/-45]_s$ graphite/epoxy panel.

layers, are attributed to the partial coverage of the surface by piezoelectric patches and the averaging of electric potential occurring on each piezoceramic because of the finite size of their continuous electrodes. Besides demonstrating the extreme capabilities of the developed methodology, the results show that the technique can yield substantial damping increases for select modes, provided that the shunting resistance, size, and location of the piezoelectric layers is properly designed. The value of the developed mechanics and FEM in accomplishing such design tasks is apparent.

Conclusions

A formulation was described for predicting the damped dynamic characteristics of laminated composite shell structures with piezoelectric layers connected to distributed passive electric networks. The formulation includes multifield mechanics for curvilinear piezoelectric laminates having distributed passive electric components. Finite element based mechanics and an eight-node specialty shell element for predicting the modal damping, modal frequencies, and damped response of piezoelectric shells were also formulated and encoded into research software.

Experimental and numerical studies illustrated the quality of the formulation and quantified the concept of passive piezoelectric damping on various structural configurations. The modal damping and frequencies of a composite beam with a variable resistor-piezoceramic element were measured and correlated with predicted results. Additional correlations with exact in-plane solutions for plates and shells illustrated the fast convergence of the developed finite element. The modal damping and frequency of cylindrical composite blades with resistively shunted curved piezoelectric patches were also predicted. All analytical and experimental studies have shown that, regardless of the structural configuration, 1) the concept of passive piezoelectric damping is feasible and 2) the damping can be easily tuned by changing the resistance value and reach a peak at an optimal resistance value that differs for each node. The shape of the structure seems to affect drastically the maximum damping value of each mode, with curvature effects being predominant. The finite size and location of piezoelectric elements also seem to affect the damping of each mode. Application of the technique on complex structural configurations can require careful design considerations. Overall, the results have illustrated the validity and effectiveness of the developed finite element formulation for analyzing and designing passively damped piezoelectric structures.

Appendix: Piezoelectric Laminate Shell Theory

Material Tensors

Stiffness $[C]$, electric permittivity $[\varepsilon]$, and piezoelectric $[d]$ or $[e]$ tensors, respectively:

$$[C] = \begin{bmatrix} C_{11} & C_{12} & 0 & 0 & C_{16} \\ \cdot & C_{22} & 0 & 0 & C_{26} \\ \cdot & \cdot & C_{44} & C_{45} & 0 \\ \cdot & \cdot & \cdot & C_{55} & 0 \\ \cdot & \cdot & \cdot & \cdot & C_{66} \end{bmatrix}, \qquad [\varepsilon] = \begin{bmatrix} \varepsilon_{11} & 0 & 0 \\ \cdot & \varepsilon_{22} & 0 \\ \cdot & \cdot & \varepsilon_{33} \end{bmatrix}$$

$$[d]^T = \begin{bmatrix} 0 & 0 & d_{31} \\ 0 & 0 & d_{32} \\ 0 & 0 & d_{33} \\ d_{14} & d_{24} & 0 \\ d_{15} & d_{25} & 0 \\ 0 & 0 & d_{36} \end{bmatrix}, \qquad [e] = [d][C]$$

Generalized Compatibility Equations

Strain and curvature vectors $\boldsymbol{S}^o$ and k, respectively[10]:

$$\boldsymbol{S}_1^o = \frac{1}{g_{11}^o}\left(u_{,\xi}^o + \frac{g_{11,\eta}^o}{g_{22}^o}v^o\right) + \frac{w^o}{R_1}$$

$$\boldsymbol{S}_2^o = \frac{1}{g_{22}^o}\left(v_{,\eta}^o + \frac{g_{22,\xi}^o}{g_{11}^o}u^o\right) + \frac{w^o}{R_2}$$

$$\boldsymbol{S}_6^o = \frac{1}{g_{11}^o}\left(v_{,\xi}^o - \frac{g_{11,\eta}^o}{g_{22}^o}u^o\right) + \frac{1}{g_{22}^o}\left(u_{,\eta}^o - \frac{g_{22,\xi}^o}{g_{11}^o}v^o\right)$$

$$\boldsymbol{S}_4^o = \beta_\eta + \frac{w_{,\eta}^o}{g_{22}^o} - \frac{v^o}{R_2}, \qquad \boldsymbol{S}_5^o = \beta_\xi + \frac{w_{,\xi}^o}{g_{11}^o} - \frac{u^o}{R_1} \tag{A1}$$

$$k_1 = \frac{1}{g_{11}^o}\left(\beta_{\xi,\xi} + \frac{g_{11,\eta}^o}{g_{22}^o}\beta_\eta\right), \qquad k_2 = \frac{1}{g_{22}^o}\left(\beta_{\eta,\eta} + \frac{g_{22,\xi}^o}{g_{11}^o}\beta_\xi\right)$$

$$k_6 = \frac{1}{g_{11}^o}\left(\beta_{\eta,\xi} - \frac{g_{11,\eta}^o}{g_{22}^o}\beta_\xi\right) + \frac{1}{g_{22}^o}\left(\beta_{\xi,\eta} - \frac{g_{22,\xi}^o}{g_{11}^o}\beta_\eta\right) \tag{A2}$$

Electric field components:

$$\boldsymbol{E}_i(\xi, \eta, \zeta, t) = \sum_{m=1}^{N} \boldsymbol{E}_i^m(\xi, \eta, t)\Psi^m(\zeta), \qquad i = 1, 2$$

$$\boldsymbol{E}_3(\xi, \eta, \zeta, t) = \sum_{m=1}^{N} \boldsymbol{E}_3^m(\xi, \eta, t)\Psi_{,\zeta}^m(\zeta) \tag{A3}$$

and generalized electric field vectors $\{\boldsymbol{E}^m\}$:

$$\boldsymbol{E}_1^m = -\frac{\Phi^m_{,\xi}}{g^o_{11}}, \qquad \boldsymbol{E}_2^m = -\frac{\Phi^m_{,\eta}}{g^o_{22}}, \qquad \boldsymbol{E}_3^m = -\Phi^m \tag{A4}$$

Laminate Matrices

Stiffness matrices $[A]$, $[B]$, and $[D]$:

$$\langle A_{ij}, B_{ij}, D_{ij}\rangle = g^o_{11}g^o_{22}\sum_{l=1}^{L}\int_{\zeta_l}^{\zeta_{l+1}} C_{ij}\langle 1, \zeta, \zeta^2\rangle \,\mathrm{d}\zeta, \quad i, j = 1, 2, 6$$

$$A_{ij} = g^o_{11}g^o_{22}\sum_{l=1}^{L}\int_{\zeta_l}^{\zeta_{l+1}} C_{ij}\,\mathrm{d}\zeta, \qquad i, j = 4, 5 \tag{A5}$$

Piezoelectric matrices $[\bar{E}^m]$ and $[\hat{E}^m]$:

$$\langle \bar{E}^m_{ij}, \hat{E}^m_{ij}\rangle = g^o_{11}g^o_{22}\sum_{l=1}^{L}\int_{\zeta_l}^{\zeta_{l+1}} e_{ij}\Psi^m_{,\zeta}(\zeta)\langle 1, \zeta\rangle \,\mathrm{d}\zeta \qquad i = 3, \quad j = 1, 2, 6$$

$$\bar{E}^m_{ij} = g^o_{11}g^o_{22}\sum_{l=1}^{L}\int_{\zeta_l}^{\zeta_{l+1}} e_{ij}\Psi^m(\zeta)\,\mathrm{d}\zeta, \qquad i = 1, 2, \quad j = 4, 5 \tag{A6}$$

and matrices of electric permittivity $[G^{mn}]$:

$$G^{mn}_{ii} = g^o_{11}g^o_{22}\sum_{l=1}^{L}\int_{\zeta_l}^{\zeta_{l+1}} \varepsilon_{ii}\Psi^m(\zeta)\Psi^n(\zeta)\,\mathrm{d}\zeta, \qquad i = 1, 2$$

$$G^{mn}_{33} = g^o_{11}g^o_{22}\sum_{l=1}^{L}\int_{\zeta_l}^{\zeta_{l+1}} \varepsilon_{33}\Psi^m_{,\zeta}(\zeta)\Psi^n_{,\zeta}(\zeta)\,\mathrm{d}\zeta \tag{A7}$$

where $(N-1)$ is the number of discrete layers and L is the number of plies in the laminate. All remaining matrix terms not shown in the preceding equations are zero.

Acknowledgments

Most of this work was performed at the Machine Dynamics Branch, Structures and Acoustics Division of NASA John H. Glenn Research Center at Lewis Field and was funded by NASA Cooperative Agreement NCC3-455. Dale A. Hopkins was the contract monitor. This support is gratefully acknowledged.

References

[1] Crawley, E. F., "Intelligent Structures for Aerospace: A Technology Overview and Assessment," *AIAA Journal*, Vol. 32, No. 8, 1994, pp. 1689–1699.

[2] Rao, S. S., and Sunar, M., "Piezoelectricity and Its Use in Disturbance Sensing and Control of Flexible Structures: A Survey," *Applied Mechanics Reviews*, Vol. 47, No. 4, 1994, pp. 113–123.

[3] Hagood, N. W., and von Flotow, A. H., "Damping of Structural Vibrations with Piezoelectric Materials and Passive Electrical Networks," *Journal of Sound and Vibration*, Vol. 146, No. 2, 1991, pp. 243–268.

[4] Law, H. H., Rossiter, P. L., Simon, G. P., and Koss, L. L., "Characterization of Mechanical Vibration Damping by Piezoelectric Materials," *Journal of Sound and Vibration*, Vol. 197, No. 4, 1996, pp. 489–513.

[5] Davis, C. L., and Lesieutre, G. A., "A Modal Strain-Energy Approach to the Prediction of Resistively Shunted Piezoceramic Damping," *Journal of Sound and Vibration*, Vol. 184, No. 1, 1995, pp. 129–139.

[6] Koshigoe, S., and Murdock, J. W., "A Unified Analysis of Both Active and Passive Damping for a Plate with Piezoelectric Transducers," *Journal of the Acoustical Society of America*, Vol. 93, No. 1, 1993, pp. 346–355.

[7] Wang, K. W., Lai, J. S., and Yu, W. K., "An Energy Based Parametric Control Approach for Structural Vibration Suppression via Semi-Active Piezoelectric Networks," *Journal of Vibration and Acoustics*, Vol. 118, No. 3, 1996, pp. 505–509.

[8] Yarlagadda, S., Lesieutre, G. A., Yoshikawa, S., and Withnam, J., "Resistively Shunted Piezocomposites for Passive Vibration Damping," *Proceedings of the 37th AIAA/ASME/ASCE/AHS/ASC Structures, Structural Dynamics, and Materials Conference and Adaptive Structures Forum*, AIAA, Reston, VA, 1996, pp. 217–227.

[9] Saravanos, D. A., "Damped Vibration of Composite Plates with Passive Piezoelectric-Resistor Elements," *Journal of Sound and Vibration*, Vol. 221, No. 5, 1999, pp. 867–885.

[10] Saravanos, D. A., "Coupled Mixed-Field Laminate Theory and Finite Element for Smart Piezoelectric Composite Shell Structures," *AIAA Journal*, Vol. 35, No. 8, 1997, pp. 1327–1333.

A. Berman
Associate Editor